



# Metal–organic framework-derived carbon coated Ni–In intermetallic compounds for in-situ selective hydrogenation of methyl palmitate to hexadecanol in aqueous phase using methanol as hydrogen donor

Zhongze Wang<sup>1</sup> · Haonan Shi<sup>1</sup> · Sihao Shu<sup>1</sup> · Xing Zhang<sup>1</sup> · Shangzhen Feng<sup>1</sup> · Jixiang Chen<sup>1</sup>

Received: 9 April 2023 / Accepted: 11 June 2023 / Published online: 16 June 2023  
© Akadémiai Kiadó, Budapest, Hungary 2023

## Abstract

A series of Ni<sub>x</sub>In<sub>y</sub>-BTC metal organic frameworks (x/y denotes the Ni/In atomic ratio) were prepared through the solvothermal method, and then carbonized at 400–700 °C in a N<sub>2</sub> flow followed by the H<sub>2</sub> reduction at 550 °C to prepare carbon-coated Ni–In IMCs catalysts. It has been found that the H<sub>2</sub> reduction is favorable for the formation of Ni–In IMCs and the Ni–In IMCs phases in Ni<sub>x</sub>In<sub>y</sub>@C are determined by the Ni/In atomic ratio. Interestingly, a thin layer of carbon (~2 nm) coats the Ni–In IMC particles. NiIn<sub>3</sub>C<sub>0.5</sub> IMC forms in Ni<sub>2</sub>In<sub>1</sub>@C, and its crystallite size increases with carbonization temperature. In addition, raising the carbonization temperature promotes the degree of graphitization. In in-situ aqueous phase selective hydrogenation of methyl palmitate to hexadecanol using methanol as hydrogen donor, all the NiIn<sub>3</sub>C<sub>0.5</sub> IMC, NiIn IMC and Ni<sub>2</sub>In<sub>3</sub> IMC dominantly give hexadecanol, however, Ni<sub>2</sub>In<sub>3</sub> IMC is hydrothermally unstable. Therein, Ni<sub>2</sub>In<sub>1</sub>@C carbonized at 600 °C (i.e., Ni<sub>2</sub>In<sub>1</sub>@C-600/550) exhibits the best performance with the hexadecanol yield of 90.3%, and the hexadecanol yield maintains ~90% during 5 times recycling. Such high activity and stability are ascribed to stable NiIn<sub>3</sub>C<sub>0.5</sub> IMC phase, thin carbon layer and suitable degree of graphitization in Ni<sub>2</sub>In<sub>1</sub>@C-600/550.

**Keywords** Ni–In-BTC MOFs · Carbon-coated Ni–In IMCs · In-situ selective hydrogenation in aqueous phase · Methyl palmitate · Hexadecanol · Hydrothermal stability

---

✉ Jixiang Chen  
jxchen@tju.edu.cn

<sup>1</sup> Tianjin Key Laboratory of Applied Catalysis Science and Technology, Department of Catalysis Science and Engineering, School of Chemical Engineering and Technology, Tianjin University, Tianjin 300350, China

## Introduction

Traditional fossil fuels are non-renewable and their extensive application poses significant environmental concerns, and there has been a marked increase in interest in utilizing renewable energy sources over the past decade [1]. Biomass is the only realistic renewable carbon resource [2]. Particularly, triglyceride fatty acids in vegetable oils/ animal fatty can be transformed into bio-diesel [3, 4] and fatty alcohols [5, 6] through hydrodeoxygenation and selective hydrogenation, respectively.

Fatty alcohols are important chemical intermediates. Cu/Cr catalysts are commonly employed for the selective hydrogenation of fatty acids/esters to produce fatty alcohols [7]. However, the loss of Cr results in environmental concern. Metallic Ni has garnered significant attention due to its low cost and high activity for hydrogenation. Unfortunately, metallic Ni is also highly active for decarbonylation/decarboxylation (DeCO/DeCO<sub>2</sub>), C–C bond hydrogenolysis and methanation [8], which are detrimental to producing fatty alcohols. This problem can be overcome by incorporating a second oxygenophilic metal to metallic Ni lattice forming alloys or intermetallic compounds (IMCs). For example, Kong et al [9] have investigated the selective hydrogenation of stearic acid on Ni<sub>3</sub>Fe IMC catalyst, where the stearic alcohol yield reaches 98%. Wang et al. [10] have found that SiO<sub>2</sub>-loaded Ni–In IMCs catalysts dominantly give octanol in the selective hydrogenation of methyl caprylate and suggested that there is a synergistic interaction between Ni and In.

Selective hydrogenation is commonly carried out under external H<sub>2</sub> that is mainly produced from the fossil fuels. Also, there are high-cost and safety problems during the H<sub>2</sub> storage and transportation. To circumvent it, the coupling of H<sub>2</sub> production and selective hydrogenation (i.e., in-situ hydrogenation) is promising, especially the H<sub>2</sub> production via aqueous phase reforming (APR) [11, 12]. Recently, Gou et al. [13] have investigated the performance of CuCo/C catalysts for in-situ hydrogenation of lauric acid in aqueous phase with methanol as a hydrogen donor, and the lauryl alcohol yield reaches 62.3% at 330 °C. It should be noticed that the harsh hydrothermal condition leads to the catalyst deactivation due to sintering [14], leaching [15], and phase transformation [16]. Supporting metals on hydrothermally stable supports (such as TiO<sub>2</sub> and ZrO<sub>2</sub>) can enhance the catalyst stability. Zhang et al. [17] have found that Cu–Ni/ZrO<sub>2</sub> maintains a relatively stable activity in in-situ aqueous phase hydrodeoxygenation of oleic acid into heptadecane at 350 °C even after being used three times.

Recently, the metals coated by hydrothermally stable carbon have gained great attention since the physical confinement of carbon can limit the sintering and leaching of active metals. The carbon-coated catalysts can be prepared from a variety of carbon sources, such as phenol–formaldehyde resins [18], biomass (such as glucose and cellulose) [19, 20], and metal–organic frameworks (MOFs) [21]. For instance, Shi et al. [22] have prepared carbon-coated Ni–Co alloy catalysts through the carbonization of Ni–Co doped phenol–formaldehyde resins, which give the n-C<sub>6</sub> ~ n-C<sub>16</sub> yield of 92.6% at 330 °C in the aqueous phase

deoxygenation of methyl palmitate, and there is no remarkable sintering and leaching of Ni–Co alloy during the reaction. Similarly, the carbon-coated Ni–Sn IMCs catalysts derived from the carbonization of Ni and Sn doped phenol–formaldehyde resins give the n-C<sub>15</sub> yield of 88.1% at 330 °C [23]. Particularly, the carbon-encapsulated Ni–Sn IMCs catalysts show good stability. Gu et al. [24] have prepared the carbon-coated Ni–In IMCs catalysts through a hydrothermal method combined with carbonization using glucose as a carbon source, which demonstrate remarkable resistance to sintering and leaching under harsh hydrothermal condition. In in-situ aqueous phase selective hydrogenation of methyl palmitate, the yield of hexadecanol reaches 81.3% at 330 °C. Unfortunately, the as-prepared Ni–In IMCs are readily deactivated due to carbonaceous deposit that blocks the pores.

Metal–organic frameworks (MOFs) are a newly emerging class of materials with a periodic network structure composed of organic linkers and metal clusters. MOFs-derived carbon-coated catalysts possess numerous advantages [21, 25, 26]: (I) the diversity of organic linkers and metal clusters, as well as the connection between them, make MOFs-derived carbon-coated catalysts more designable. (II) The alternating distribution of ligands and metal results in a uniform distribution of metal in MOFs-derived carbon-coated catalysts. (III) MOFs possess high surface area and porosity. (IV) MOFs can be easily prepared with mild condition, and so on. Bimetallic MOFs can be fabricated by various methods, such as one-pot synthesis, impregnation, and metal ion exchange [27]. The one-pot method offers a simple process, good repeatability and uniformity. 1,3,5-Benzenetricarboxylic acid (BTC) is widely used as organic linker and can coordinate with many metals (such as Ni [28, 29] and In [30, 31]) to form MOFs. Liu et al. [32] have prepared Ni@C-BTC from Ni-BTC MOFs through carbonization under a N<sub>2</sub> atmosphere, which exhibits high activity and stability in the hydrodeoxygenation of triolein. Under reaction conditions of 320 °C, 3 MPa H<sub>2</sub> and 4 h, the conversion of fatty acid reaches 98.9% with 4.6% cracking ratio. Although the carbon-coated structure suppresses the catalyst deactivation due to sintering and leaching, it may give rise to internal diffusion limitation and thus is harmful to the catalyst activity. Inspired from previous works [33], a feasible strategy is to reduce the thickness of the carbon layer and increase the proportion of mesoporous. MOFs are porous and have a thin carbon layer in their derived carbon materials [34]. As mentioned in previous works [10, 21], Ni–In IMCs are very promising for the selective hydrogenation of fatty acids/esters to fatty alcohols, and the carbon coating can effectively limit the sintering and leaching of metals in catalysts, we speculate that coated Ni–In IMCs derived from MOFs may give the catalysts with high performance. To the best of our knowledge, no Ni–In-BTC MOFs and their derived Ni–In IMC@C catalysts have been reported in the literature.

In the present study, bimetallic Ni–In-BTC MOFs were synthesized by the one-pot solvothermal method, and then converted to the carbon-coated Ni–In IMCs catalysts through the carbonization in the N<sub>2</sub> atmosphere followed by H<sub>2</sub> reduction. The as-prepared catalysts were tested for the aqueous phase selective hydrogenation of methyl palmitate using methanol as a hydrogen donor. Interestingly, the as-prepared catalyst gave the hexadecanol yield of ~90% and showed

good stability. The relationship between the catalyst structure and performance was also explored.

## Experimental

### Materials

All reagents were purchased without any further purification.  $\text{Ni}(\text{NO}_3)_2 \cdot 6\text{H}_2\text{O}$  was purchased from Adamas-beta Co., Ltd.  $\text{In}(\text{NO}_3)_3 \cdot 4\text{H}_2\text{O}$  was purchased from Guangxi Shimei Ceramic Products Co., Ltd. 1,3,5-Benzene tricarboxylate (BTC), Ethyl palmitate, Octadecane and Tetralin were purchased from Aladdin Bio-Chem Technology Co., Ltd. Methanol was purchased from Kermel Co., Ltd. *N,N*-dimethylformamide (DMF) was purchased from Meryer Co., Ltd. Ethanol, Cyclohexane and Ethyl acetate were purchased from Real & Lead Chemical Co., Ltd.

### Catalyst preparation

#### Synthesis of Ni-BTC, In-BTC and $\text{Ni}_x\text{In}_y\text{-BTC}$

Ni-BTC, In-BTC and  $\text{Ni}_x\text{In}_y\text{-BTC}$  MOFs (where  $x/y$  denote the nominal Ni/In atomic ratio) were prepared by the solvothermal method [27].  $\text{Ni}(\text{NO}_3)_2 \cdot 6\text{H}_2\text{O}$ ,  $\text{In}(\text{NO}_3)_3 \cdot 4\text{H}_2\text{O}$  and BTC (the amounts are listed in Table 1) were dissolved in 60 mL DMF. The solution was then sealed in a 100 mL Teflon-lined stainless-steel autoclave and heated to 120 °C maintained for 24 h. Afterward, the solid was centrifuged, washed 3–4 times with ethanol, and dried overnight at 80 °C. The resulting MOFs are named as  $\text{Ni}_x\text{In}_y\text{-BTC}$ . Ni-BTC and In-BTC were prepared using the same procedure.

#### Synthesis of $\text{Ni}_x\text{In}_y\text{@C}$ catalysts

$\text{Ni}_x\text{In}_y\text{-BTC}$  MOFs were carbonized in a  $\text{N}_2$  flow at different temperatures for 2 h on a fixed-bed quartz reactor (0.8 cm in diameter), and the resulting catalysts are

**Table 1** The mass of raw material

Catalyst	The amount of raw material addition (g)		
	$\text{Ni}(\text{NO}_3)_2 \cdot 6\text{H}_2\text{O}$	$\text{In}(\text{NO}_3)_3 \cdot 4\text{H}_2\text{O}$	BTC
Ni-BTC	5.82	0	4.203
$\text{Ni}_2\text{In}_1\text{-BTC}$	3.877	2.486	4.203
$\text{Ni}_1\text{In}_1\text{-BTC}$	2.910	3.728	4.203
$\text{Ni}_2\text{In}_3\text{-BTC}$	2.326	4.474	4.203
$\text{Ni}_1\text{In}_2\text{-BTC}$	1.939	4.971	4.203
$\text{Ni}_1\text{In}_3\text{-BTC}$	1.454	5.592	4.203
In-BTC	0	7.457	4.203

denoted as Ni<sub>x</sub>In<sub>y</sub>@C-T (where T indicates the carbonization temperature). The as-prepared Ni<sub>x</sub>In<sub>y</sub>@C-T catalysts were further reduced by a H<sub>2</sub> flow at 550 °C for 1 h and named as Ni<sub>x</sub>In<sub>y</sub>@C-T/550. Before exposure to air, the reduced catalysts were passivated at room temperature with a 0.5% O<sub>2</sub>/N<sub>2</sub> flow (320 mL/min) for 2 h.

### Catalyst characterization

The X-ray diffraction (XRD) pattern was acquired on a D8 X-ray diffractometer with Cu K<sub>α</sub> radiation ( $\lambda=0.1541$  nm). Transmission electron microscopy (TEM) and scanning electron microscopy (SEM) were performed using JEM-F200 field-emission electron microscope and Hitachi s-4800 instruments. Raman spectra were recorded on a LabRAM HR Evolution. N<sub>2</sub> physisorption isotherms were measured on a Quantachrome Autosorb at  $-196$  °C. Specific surface area (S<sub>BET</sub>) was determined by the Brunauer–Emmett–Teller (BET) equation. The Horvath–Kawazoe method was applied to determine micropore volume (V<sub>mic</sub>) and micropore diameter (d<sub>mic</sub>), and the mesopore volume (V<sub>mes</sub>) and mesopore diameter (d<sub>mes</sub>) were calculated by the Barrett–Joyner–Halenda (BJH) equation.

### Catalytic test

The in-situ aqueous phase selective hydrogenation of methyl palmitate was tested using a 100 mL batch reactor (Beijing Century Senlong Experimental Apparatus Co., Ltd.). Firstly, 4 g of methyl palmitate, 8 g of deionized water, 3 g of methanol and 0.4 g of catalyst were charged into the reactor. After the reactor was sealed, it was purged with N<sub>2</sub> for three times to replace air and then pressurized with N<sub>2</sub> to 1.0 MPa. The reactor was heated to set temperature under stirring at 500 rpm. After the reaction, the reactor was cooled down to 50 °C by internal cooling water system. The organic components were extracted using cyclohexane.

The organic products were analyzed using a SP-3420 gas chromatograph (GC) equipped with an HP-5 capillary column and a flame ionization detector (FID). For the organic phase, ethyl acetate and tetralin were used as the internal standard to analyze methanol and n-C<sub>6</sub>~n-C<sub>14</sub> alkanes, while octadecane was used as the internal standard to analyze pentadecane, hexadecane, hexadecanal, hexadecanol, palmitic acid, and methyl palmitate. Methanol in aqueous phase was analyzed using ethanol as internal standard. The conversions of methyl palmitate and methanol and the yield of different products were calculated using the following equations:

$$\text{Conversion (\%)} = 1 - \frac{\text{mole of unreacted methyl palmitate}}{\text{mole of methyl palmitate added}} \times 100\%$$

$$\text{Yield (\%)} = 1 - \frac{\text{mole of product} \times \text{carbon atom number in product}}{\text{mole of methyl palmitate added} \times 16} \times 100\%$$

All the tests were repeated 2–3 times. The error range is within  $\pm 6\%$  and the standard deviation is no more than 4%.

## Results and discussion

### Catalyst characterization

#### Ni-BTC, Ni<sub>x</sub>In<sub>y</sub>-BTC and In-BTC MOFs

Fig. 1 shows the XRD patterns of Ni-BTC, In-BTC and Ni<sub>x</sub>In<sub>y</sub>-BTC. The XRD pattern of Ni-BTC is similar to that in the literature [32], indicative of the successful preparation of Ni-BTC MOF. In contrast, In-BTC shows a completely different XRD pattern from Ni-BTC, i.e., forming a distinct crystal. In-BTC is dominating in Ni<sub>1</sub>In<sub>3</sub>-BTC. For Ni<sub>x</sub>In<sub>y</sub>-BTC with higher Ni/In atomic ratios (i.e., Ni<sub>1</sub>In<sub>2</sub>-BTC, Ni<sub>2</sub>In<sub>3</sub>-BTC, and Ni<sub>1</sub>In<sub>1</sub>-BTC), the peaks due to both In-BTC and Ni-BTC are observed. This indicates that Ni<sub>1</sub>In<sub>2</sub>-BTC, Ni<sub>2</sub>In<sub>3</sub>-BTC and Ni<sub>1</sub>In<sub>1</sub>-BTC are a mixture of In-BTC and Ni-BTC. Interestingly, Ni<sub>2</sub>In<sub>1</sub>-BTC exhibits a unique XRD pattern, indicating that Ni<sub>2</sub>In<sub>1</sub>-BTC is composed of a new crystal structure that is different from In-BTC and Ni-BTC. A similar phenomenon has also been reported by Zhang et al. [35].

The morphologies and structures of Ni-BTC, Ni<sub>x</sub>In<sub>y</sub>-BTC and In-BTC are studied by SEM. As depicted in Fig. S1, Ni-BTC displays a prismatic block with interspersed irregular particles. The Ni<sub>2</sub>In<sub>1</sub>-BTC sample exhibits a regular hexagonal block structure with a particle size of approximately 5 μm. Ni<sub>1</sub>In<sub>1</sub>-BTC shows a large number of irregular particles in addition to hexagonal blocks, with agglomerations between the particles. The overall shape of Ni<sub>2</sub>In<sub>3</sub>-BTC closely resembles that of Ni<sub>2</sub>In<sub>1</sub>-BTC but displays a lamellar structure. Ni<sub>1</sub>In<sub>2</sub>-BTC and Ni<sub>1</sub>In<sub>3</sub>-BTC exhibit irregularly blocky with agglomeration. The In-BTC sample exhibits a trigonal structure.

TEM images (Fig. S2) show that Ni<sub>2</sub>In<sub>1</sub>-BTC presents a crystal structure. The large size of the Ni<sub>2</sub>In<sub>1</sub>-BTC particles (about 5 μm) is consistent with that from the

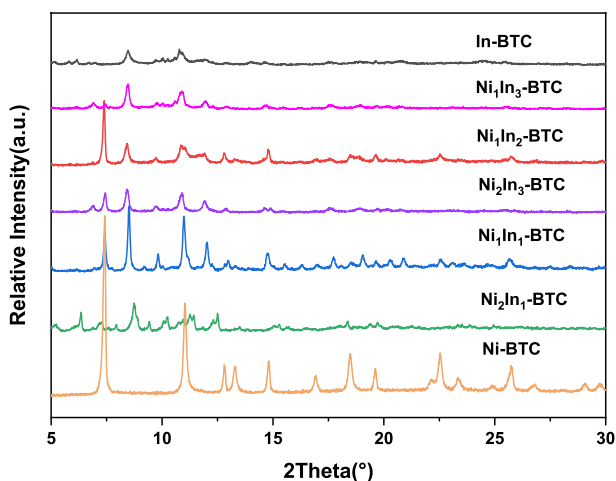
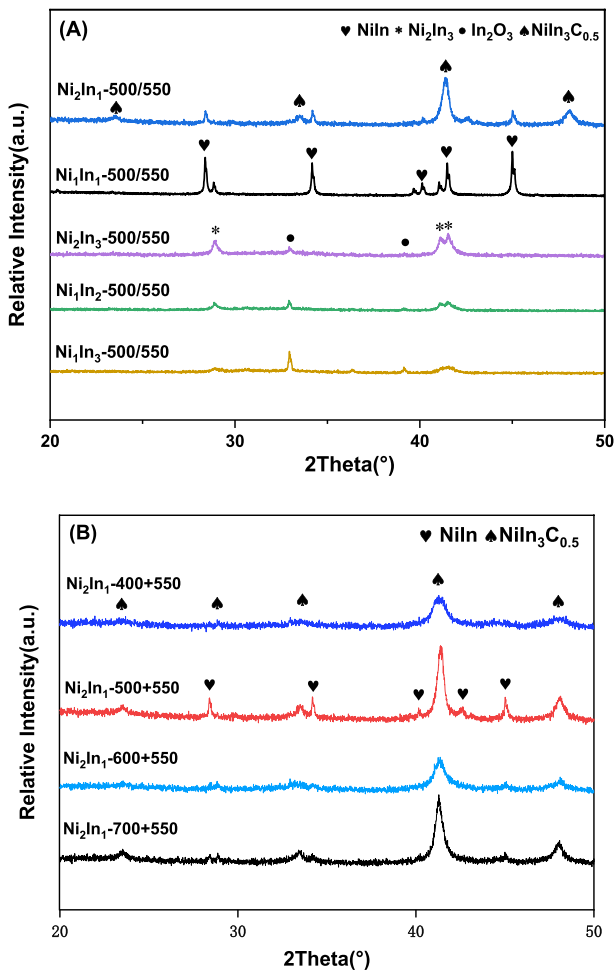


Fig. 1 XRD patterns of Ni-BTC, In-BTC, and Ni<sub>x</sub>In<sub>y</sub>-BTC

SEM images. As shown by the TEM-EDS mapping scanning of  $\text{Ni}_2\text{In}_1\text{-BTC}$ , In, Ni and C elements uniformly distribute in the particle, which is favorable for the formation of carbon-coated Ni–In IMCs as indicated below.

### $\text{Ni}_x\text{In}_y\text{@C}$ catalyst derived from MOFs

The preliminary exploration indicates that the  $\text{In}_2\text{O}_3$  phase without reduction during the carbonization can be reduced by  $\text{H}_2$  at 550 °C, which is favorable for the formation of Ni–In IMCs (see Fig. S3A). Based on this, the  $\text{Ni}_x\text{In}_y\text{@C-500/550}$  catalysts with different Ni/In atomic ratios were prepared. As shown in Fig. 2A,  $\text{NiIn}_3\text{C}_{0.5}$  IMC (PDF#28-0468) is dominating in  $\text{Ni}_2\text{In}_1\text{@C-500/550}$ , accompanied with minor NiIn IMC (PDF#07-0178). For  $\text{Ni}_1\text{In}_1\text{@C-500/550}$ , the diffraction peaks



**Fig. 2** XRD patterns of different catalysts. **A**  $\text{Ni}_x\text{In}_y\text{@C-500/550}$ ; **B**  $\text{Ni}_2\text{In}_1\text{@C-T/550}$

attributed to NiIn IMC and  $\text{Ni}_2\text{In}_3$  IMC are visible. There is main  $\text{Ni}_2\text{In}_3$  IMC in  $\text{Ni}_2\text{In}_3@\text{C-500/550}$ ,  $\text{Ni}_1\text{In}_2@\text{C-500/550}$  and  $\text{Ni}_1\text{In}_3@\text{C-500/550}$ , and the peaks attributed to  $\text{In}_2\text{O}_3$  (PDF # 06-0416) become sharp with the increase of In content.

As shown in Fig. 2B,  $\text{Ni}_2\text{In}_1@\text{C-T/550}$  derived from different carbonization temperatures exhibit similar XRD patterns, and all the catalysts contain  $\text{NiIn}_3\text{C}_{0.5}$  IMC. Based on the Scherrer equation, the crystallite sizes of  $\text{NiIn}_3\text{C}_{0.5}$  IMC are estimated to be 7.4, 9.6, 11.4 and 15.4 nm in  $\text{Ni}_1\text{In}_1@\text{C-400/550}$ ,  $\text{Ni}_1\text{In}_1@\text{C-500/550}$ ,  $\text{Ni}_1\text{In}_1@\text{C-600/550}$  and  $\text{Ni}_1\text{In}_1@\text{C-700/550}$ . That is, raising the carbonization temperature promotes the sintering of  $\text{NiIn}_3\text{C}_{0.5}$  IMC particles.

$\text{Ni}_x\text{In}_y\text{-BTC}$  MOFs are carbonized at different temperatures, and their morphology is not obviously influenced by the carbonization process (Fig. S4), similar to the previous reports [36–38]. Fig. 3 shows TEM and HRTEM images of  $\text{Ni}_2\text{In}_1@\text{C-600/550}$ . The  $\text{NiIn}_3\text{C}_{0.5}$  IMC particles uniformly disperse, and the average size is approximately 10.8 nm, approaching the XRD results in Fig. 2B.  $\text{NiIn}_3\text{C}_{0.5}$  IMC particles may correspond to the nanoparticles on the catalysts surface as shown in SEM images (Fig. S4). Same to the case in SEM image (Fig. S4), the hexagonal structure is also observed in TEM images (Fig. S5). Particularly, the HRTEM image shows that there is a very thin layer of carbon ( $\sim 2$  nm) on the surface of the  $\text{NiIn}_3\text{C}_{0.5}$  IMC particles, demonstrating that the carbon-coated Ni–In IMCs is prepared. Such the thin carbon layer is beneficial to reducing internal transfer limitation and so good catalytic performance as mentioned below.

Fig. 4 shows the Raman spectra of  $\text{Ni}_x\text{In}_y@\text{C}$ . The degree of graphitization is usually determined by the peak area ratio of D-band to G-band (i.e. the  $I_D/I_G$  ratio). The lower the  $I_D/I_G$  ratio, the higher the degree of graphitization. As shown in Fig. 4, the  $I_D/I_G$  ratios for  $\text{Ni}_2\text{In}_1@\text{C-500}$  and  $\text{Ni}_2\text{In}_1@\text{C-500/550}$  are 3.25 and 3.01y. In addition, the  $I_D/I_G$  ratios for  $\text{Ni}_2\text{In}_3@\text{C-500}$  and  $\text{Ni}_2\text{In}_3@\text{C-500/550}$  are 3.33 and 3.03. Therefore, the  $\text{H}_2$  reduction promotes the graphitization of carbon, consistent with the case in the literature [39]. Furthermore, for  $\text{Ni}_2\text{In}_3@\text{C-T/550}$ , the  $I_D/I_G$  ratios decrease from 4.31 to 2.58 with rising the carbonization temperature, i.e., the increased carbonization temperatures accelerate the graphitization, consistent with

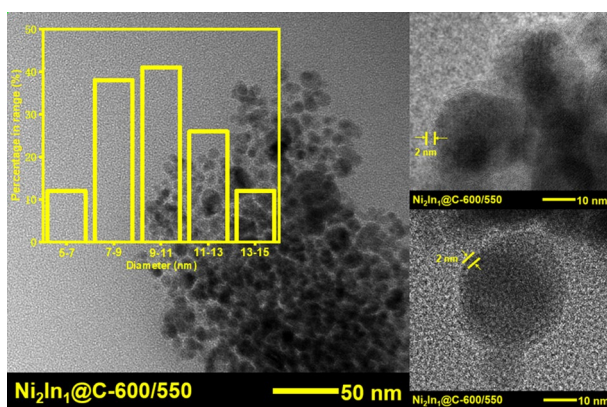
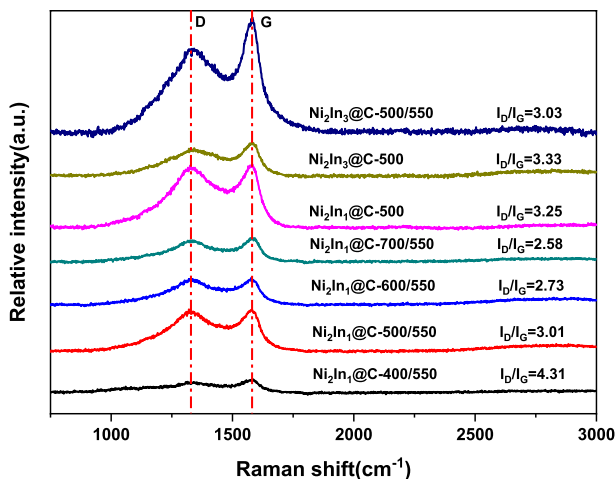


Fig. 3 TEM and HRTEM images of  $\text{Ni}_2\text{In}_1@\text{C-600/550}$





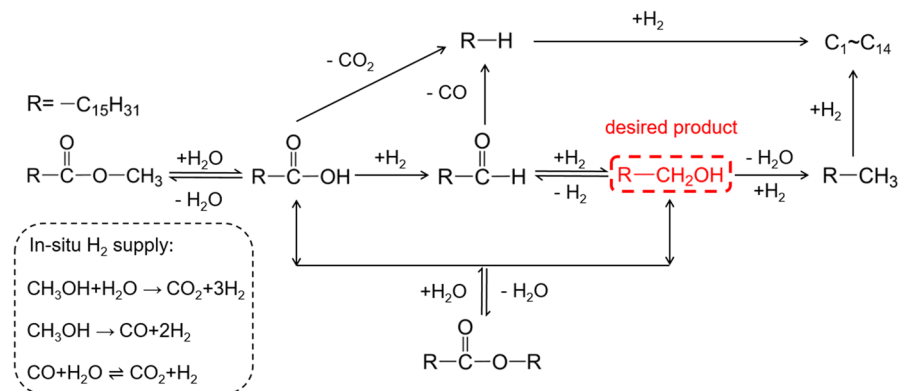
**Fig. 4** Raman spectra of  $\text{Ni}_x\text{In}_y\text{@C}$

the literature [32]. In addition,  $\text{Ni}_2\text{In}_1\text{@C-500}$  with higher Ni/In atomic ratio shows higher graphitization than  $\text{Ni}_2\text{In}_3\text{@C-500}$ .

$\text{N}_2$  adsorption–desorption isotherms of  $\text{Ni}_2\text{In}_1\text{@C-600}$ , fresh and used  $\text{Ni}_2\text{In}_1\text{@C-600/550}$  are measured. As shown in Fig. S6 and Table S1, both the pore volume and pore size of  $\text{Ni}_2\text{In}_1\text{@C-600}$  increase after the  $\text{H}_2$  reduction at  $550^\circ\text{C}$ . This can be explained by that  $\text{H}_2$  may react with the carbon species to form gaseous hydrocarbons [39]. The large pore size and pore volume favor the mass transfer during the reaction.

### Catalytic performance

The performance of carbon-coated Ni–In IMCs catalysts was tested for the in-situ selective hydrogenation of methyl palmitate to hexadecanol in the aqueous phase using methanol as hydrogen donor. Since metallic Ni is highly active for  $\text{DeCO}/\text{DeCO}_2$  and C–C bond hydrogenolysis leading to very low yield of hexadecanol [22–24], the Ni@C catalyst was not tested in this work. Based on previous work [24, 40–42] and product distribution, the in-situ selective hydrogenation pathway of methyl palmitate in aqueous phase is proposed in Scheme 1. Under the present reaction condition, methyl palmitate is readily hydrolyzed to palmitic acid and methanol [43], and the conversion of palmitic acid is key. Palmitic acid can be hydrogenated to generate hexadecanal. Hexadecanal, a very reactive intermediate, is easily converted to the desired product hexadecanol via hydrogenation pathway. Additionally,  $\text{DeCO}_2$  of palmitic acid and  $\text{DeCO}$  of hexadecanal produce  $n\text{-C}_{15}$ , while hexadecanol can undergo dehydration-hydrogenation yielding  $n\text{-C}_{16}$ ,  $n\text{-C}_{15}$  and  $n\text{-C}_{16}$  can further be transformed to short-chain alkanes through hydrogenolysis. It is possible that hexadecanol reacts with palmitic acid to produce palmityl palmitate through esterification. Here, Ni–In IMCs possess very low activity for C–C hydrogenolysis and  $\text{DeCO}/\text{DeCO}_2$  [10,



**Scheme 1** Hydroconversion pathways of methyl palmitate in aqueous phase

24]. Since the desired product is hexadecanol, the catalyst activity for the selective hydrogenation is mainly represented by the yield of hexadecanol.

### Effect of Ni/In atomic ratio on performance of $Ni_xIn_y@C-500/550$

According to relevant literature [39, 44] and preliminary exploration (Fig. S7),  $H_2$  reduction can promote the formation of Ni–In IMCs, increase the degree of graphitization, create pores as indicated above, and thus has a positive effect on the catalysts performance (the details are shown in the *Supplementary Information*). Therefore, the carbonized catalysts are all reduced by  $H_2$  in the following work. Fig. 5 shows the effect of Ni/In atomic ratio on the performances of  $Ni_xIn_y@C-500/550$ . Hexadecanol is the main product on all the  $Ni_xIn_y@C-500/550$ , and its yield first increases and then decreases as the Ni/In atomic ratio is reduced from 2/1 to 1/3.  $Ni_2In_3@C-500/550$  has the highest conversion of methyl palmitate (93.2%) and hexadecanol yield (87.3%). As indicated by XRD (Fig. S3B),  $Ni_2In_3$  IMC is detected in  $Ni_2In_3@C-500/550$ , while it is not stable and decomposes to form  $In_2O_3$  under harsh hydrothermal condition [35]. This may affect the catalytic stability of  $Ni_2In_3@C-500/550$ . Therefore, the stability of  $Ni_2In_1@C-500/550$  and  $Ni_2In_3@C-500/550$  were tested.

As shown in Fig. S8,  $Ni_2In_1@C-500/550$  exhibits higher catalytic stability than  $Ni_2In_3@C-500/550$ . The yield of hexadecanol is similar (~76%) on the fresh and used  $Ni_2In_1@C-500/550$ . In contrast,  $Ni_2In_3@C-500/550$  catalyst is significantly deactivated at the first recycling, and the hexadecanol yield decreases from 87.3 to 47.5%. The hydrothermal instability of  $Ni_2In_3$  IMC may account for its deactivation. Thus,  $Ni_2In_1@C$  containing stable  $NiIn_3C_{0.5}$  IMC is preferential for in-situ selective hydrogenation of methyl palmitate to hexadecanol.

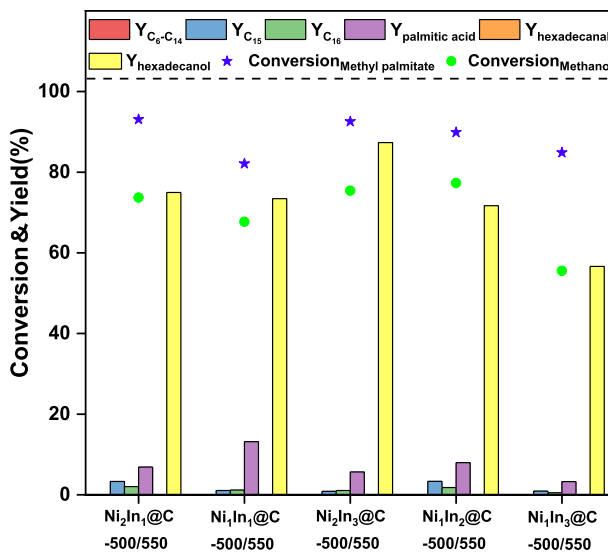


**Fig. 5** Performance of  $Ni_xIn_y@C-500/550$  for in-situ selective hydrogenation of methyl palmitate in aqueous phase using methanol as hydrogen donor. Reaction condition: 4 g methyl palmitate, 3 g methanol, 8 g water, 0.4 g catalyst, 330 °C, 1 h

### Effect of carbonation temperature on performance of $Ni_2In_1@C-T/550$

The effect of carbonation temperature on performance of  $Ni_2In_1@C-T/550$  is depicted in Fig. 6. The catalysts performance first increases and then decreases with increasing carbonization temperature, and the hexadecanol yields are 68.8%, 75.6%, 81.6% and 65.5% at the carbonation temperatures of 400 °C, 500 °C, 600 °C and 700 °C. Clearly,  $Ni_2In_1@C-600/550$  exhibits the best selective hydrogenation performance. As indicated by Raman spectra (Fig. 4), the increase in carbonization temperature can improve graphitization of carbon, which is beneficial for the structure stability of carbon layer. However, too high carbonization temperature leads to grow up of IMC particles and over-graphitization of catalysts (as indicated by XRD and Raman results), which may reduce the number of exposed active sites.

### Effect of reaction condition on performance of $Ni_2In_1@C-600/550$

As above mentioned,  $Ni_2In_1@C-600/550$  is preferential for in-situ selective hydrogenation of methyl palmitate in aqueous phase. The effects of the reaction temperature and time on its performance were investigated to determine a suitable reaction condition with high yield of hexadecanol.

As illustrated in Fig. 7A, the increase in reaction temperature from 310 to 350 °C enhances the conversion of methyl palmitate from 77.1 to 95.0%, and methanol conversion from 53.5 to 90.2%. This can be attributed to the endothermic hydrolysis of methyl palmitate and aqueous phase reforming of methanol. The yield of hexadecanol increases from 50.9 to 90.3%, while the yield of palmitic acid decreases from

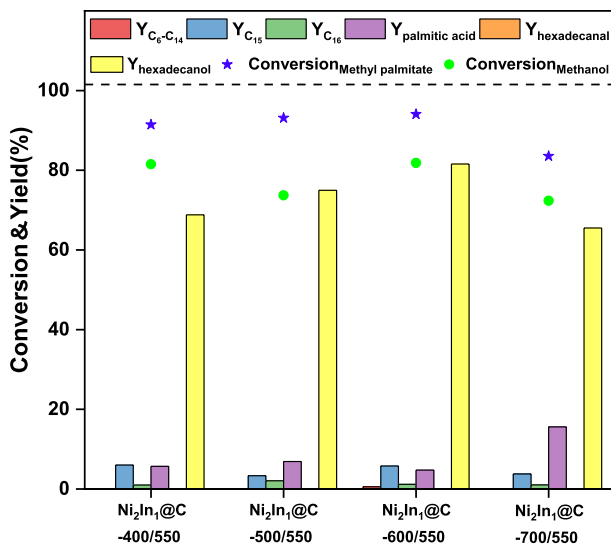


**Fig. 6** Performance of Ni<sub>x</sub>In<sub>y</sub>@C-T/550 for in-situ selective hydrogenation of methyl palmitate in aqueous phase using methanol as hydrogen donor. Reaction condition: 4 g methyl palmitate, 3 g methanol, 8 g water, 0.4 g catalyst, 330 °C, 1 h

17.7 to 3.3%. The increase in temperature enhances the H<sub>2</sub> pressure due to aqueous reforming, facilitating the selective hydrogenation of palmitic acid to hexadecanol. In addition, the yields of n-C<sub>5</sub>~n-C<sub>14</sub> alkanes are lower than 0.01%, indicating the low activity of NiIn<sub>3</sub>C<sub>0.5</sub> IMC for the C–C bond hydrogenolysis. The yields of deoxygenation products (n-C<sub>15</sub> and n-C<sub>16</sub>) increase slightly, ascribed to that the increase in temperature favors the deoxygenation and DeCO/DeCO<sub>2</sub> to produce alkanes [10, 24, 45].

As depicted in Fig. 7B, the conversion of methyl palmitate and methanol gradually increases with reaction time from 0.5 to 2 h. The yield of hexadecanol reaches the highest (90.3%) at 1 h. The conversion of hexadecanol to n-C<sub>16</sub> via dehydration-hydrogenation can account for the decrease in the yield of hexadecanol with increasing reaction time (Scheme 1).

**B** 3 g methanol, 8 g water, 0.4 g catalyst, 350 °C.

### Catalyst stability

As indicated above, Ni<sub>2</sub>In<sub>1</sub>@C-600/550 gives high hexadecanol yield. Herein, its stability was tested. Before each recycling, the catalysts were washed with isopropanol, and 0.04 g fresh catalyst was added to compensate for the catalyst loss. As shown in Fig. 8, the hexadecanol yield is 90.3% on the fresh Ni<sub>2</sub>In<sub>1</sub>@C-600/550, and it remains at approximately 90% during five times recycling, showing good stability.

The Ni<sub>2</sub>In<sub>1</sub>@C-600/550-used<sub>x</sub> catalysts (where x denotes the catalysts used after xth times) were characterized in order to account for the stability. The XRD patterns

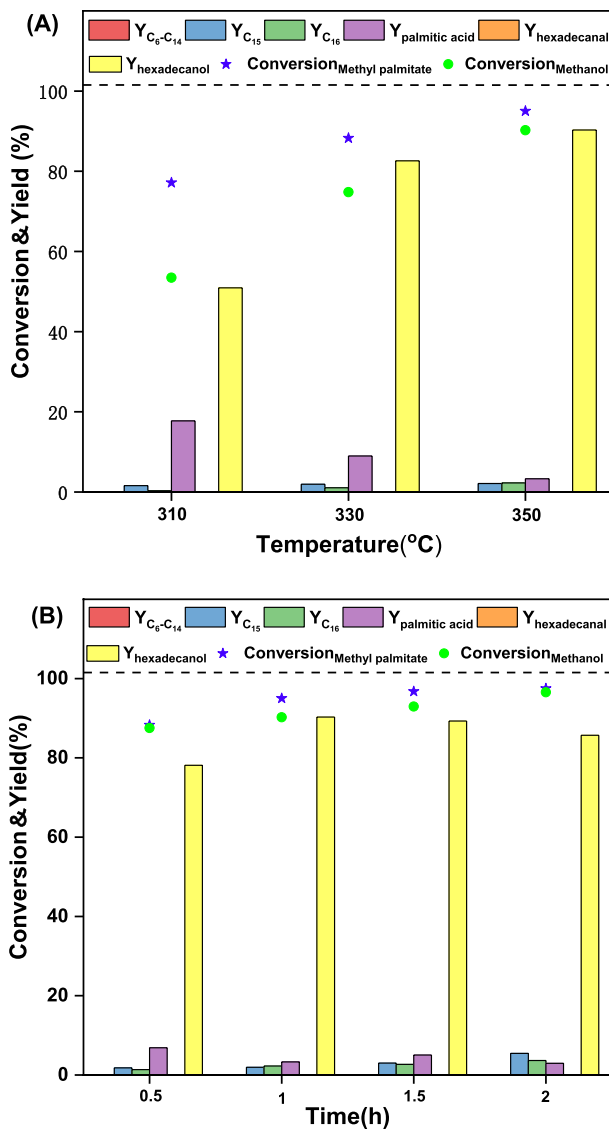


**Fig. 7** Effect of **A** reaction temperature; **B** reaction time on the performance of  $\text{Ni}_2\text{In}_1@\text{C}-600/550$  for in-situ selective hydrogenation of methyl palmitate in aqueous phase using methanol as hydrogen donor. Reaction condition: 4 g methyl palmitate, A 3 g methanol, 8 g water, 0.4 g catalyst, 1 h;

(Fig. S9) indicate that the  $\text{NiIn}_3\text{C}_{0.5}$  IMC phase is partially decomposed during the reaction for the  $\text{Ni}_2\text{In}_1@\text{C}-600/550$  catalyst because the  $\text{In}_2\text{O}_3$  phase appears after the reaction. Interestingly, there is NiIn IMC in  $\text{Ni}_2\text{In}_1@\text{C}-600/550$ -used [6]. This indicates that NiIn IMC is hydrothermally stable, consistent with the previous work [24]. The  $\text{NiIn}_3\text{C}_{0.5}$  IMC crystallite diameters on the  $\text{Ni}_2\text{In}_1@\text{C}-600/550$ ,  $\text{Ni}_2\text{In}_1@\text{C}-600/550$ -used<sub>1</sub> and  $\text{Ni}_2\text{In}_1@\text{C}-600/550$ -used<sub>6</sub> are 11.4, 13.5 and 14.9 nm,

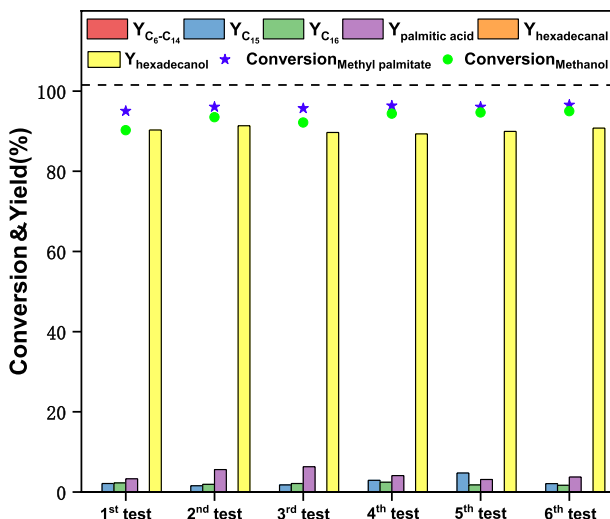


**Fig. 8** Stability of  $\text{Ni}_2\text{In}_1@\text{C-600/550}$ . Reaction condition: 4 g methyl palmitate, 3 g methanol, 8 g water, 0.4 g catalyst, 350 °C, 1 h

indicative of a slight sintering. The SEM and TEM results (Fig. S10) show that the morphology of  $\text{Ni}_2\text{In}_1@\text{C-600/550}$  is almost unchanged after the reaction, and  $\text{NiIn}_3\text{C}_{0.5}$  IMC particles is approximately 14.7 nm, consistent with the XRD results. As indicated by the results of  $\text{N}_2$  adsorption–desorption (Fig. S6, Table S1), the specific surface area ( $S_{\text{BET}}$ ) of the catalyst decreases from 182 to 128  $\text{m}^2/\text{g}$  after using for 6th times. The determine micropore volume ( $V_{\text{mic}}$ ) and mesopore volume ( $V_{\text{mes}}$ ) decrease from 0.073 and 0.196  $\text{cm}^3/\text{g}$  to 0.049 and 0.162  $\text{cm}^3/\text{g}$ , while the micropore diameter ( $d_{\text{mic}}$ ) and the mesopore diameter ( $d_{\text{mes}}$ ) do not obviously change after the reaction. This means that some pores are blocked by the carbonaceous species. Raman results show a slight increase in catalyst graphitization after five times recycling (Fig. S11). Therefore, some changes in the catalyst structure do not obviously influence the catalytic stability of  $\text{Ni}_2\text{In}_1@\text{C-600/550}$ .

In the previous work [24], the carbon-coated Ni–In IMC derived from glucose as carbon source gives the hexadecanol yield of 84% at the reaction time of 4 h, and it is deactivated in the first cycling. In contrast, MOFs derived  $\text{Ni}_2\text{In}_1@\text{C-600/550}$  has higher yield of hexadecanol (90.3%) at shorter reaction time (1 h) and good catalytic stability. This may be mainly related to the thinner carbon layer of the MOFs-derived  $\text{NiIn}@\text{C}$  catalysts. The thinner carbon layer reduces the internal diffusion limitation and so improves the catalyst activity and stability.

## Conclusion

$\text{Ni}_2\text{In}_1\text{-BTC}$  shows distinctive peaks from Ni-BTC and In-BTC.  $\text{H}_2$  reduction is favorable for the formation of Ni–In IMCs and there are  $\text{NiIn}_3\text{C}_{0.5}$ ,  $\text{NiIn}$  and  $\text{Ni}_2\text{In}_3$  IMCs forming in  $\text{Ni}_x\text{In}_y@\text{C-500/550}$  with the Ni/In atomic ratio of 2:1, 1:1 and 2:3.

Ni<sub>2</sub>In<sub>3</sub> IMC is hydrothermally unstable due to its conversion into In<sub>2</sub>O<sub>3</sub>. The crystallite sizes of NiIn<sub>3</sub>C<sub>0.5</sub> IMC and degree of graphitization raise with increased carbonization temperatures. There is a thin layer of carbon (~2 nm) on the surface of the NiIn<sub>3</sub>C<sub>0.5</sub> IMC particles. In in-situ aqueous phase selective hydrogenation of methyl palmitate to hexadecanol using methanol as hydrogen donor, Ni<sub>2</sub>In<sub>1</sub>@C-600/550 can give the best performance with the hexadecanol yield of 90.3% at the suitable condition, and it remains at approximately 90% during five times recycling. The reasons for the high activity and stability of Ni<sub>2</sub>In<sub>1</sub>@C-600/550 include: (I) Hydrothermal stable phase NiIn<sub>3</sub>C<sub>0.5</sub>, (II) suitable particle size and a certain degree of graphitization obtained by carbonization at a certain condition. (III) MOFs-derived thin carbon layer-coated structure reduces the internal diffusion limitation while retaining the physical limiting effect.

**Supplementary Information** The online version contains supplementary material available at <https://doi.org/10.1007/s11144-023-02435-7>.

**Acknowledgements** The authors gratefully acknowledge support from the National Natural Science Foundation of China (Nos. 21576193 and 21176177)

**Data availability** There is no additional data available. All other data are available from the authors upon reasonable request.

## References

1. Gallezot P (2012) Conversion of biomass to selected chemical products. *Chem Soc Rev* 41:1538–1558
2. Kim S, Kwon EE, Kim YT, Jung S, Kim HJ, Huber GW, Lee J (2019) Recent advances in hydrodeoxygenation of biomass-derived oxygenates over heterogeneous catalysts. *Green Chem* 21:3715–3743
3. Santillan-Jimenez E, Crocker M (2012) Catalytic deoxygenation of fatty acids and their derivatives to hydrocarbon fuels via decarboxylation/decarbonylation. *J Chem Technol Biotechnol* 87:1041–1050
4. Donnis B, Egeberg RG, Blom P, Knudsen KG (2009) Hydroprocessing of bio-oils and oxygenates to hydrocarbons. understanding the reaction routes. *Top Catal* 52:229–240
5. Kreutzer UR (1984) Manufacture of fatty alcohols based on natural fats and oils. *J Am Oil Chem Soc* 61:343–348
6. Turek T, Trimm D, Cant N (1994) The catalytic hydrogenolysis of esters to alcohols. *Catal Rev* 36:645–683
7. Voeste T, Buchold H (1984) Production of fatty alcohols from fatty acids. *J Am Oil Chem Soc* 61:350–352
8. Snare M, Kubickova I, Maki-Arvela P, Eranen K, Murzin DY (2006) Heterogeneous catalytic deoxygenation of stearic acid for production of biodiesel. *Ind Eng Chem Res* 45:5708–5715
9. Kong XQ, Fang ZF, Bao XB, Wang Z, Mao SJ, Wang Y (2018) Efficient hydrogenation of stearic acid over carbon coated Ni–Fe catalyst. *J Catal* 367:139–149
10. Wang L, Niu X, Chen J (2020) SiO<sub>2</sub> supported Ni–In intermetallic compounds: efficient for selective hydrogenation of fatty acid methyl esters to fatty alcohols. *Appl Catal B-Environ* 278:119293
11. Dominguez-Barroso V, Herrera C, Larrubia MA, Alemany LJ (2019) Coupling of glycerol-APR and in situ hydrodeoxygenation of fatty acid to produce hydrocarbons. *Fuel Process Technol* 190:21–28
12. Ai L, Shi YT, Han YJ, Chen JX (2021) In situ aqueous phase hydrodeoxygenation of methyl palmitate to hydrocarbons on Ni catalyst derived from the reduction of LaNiO<sub>3</sub> perovskite. *React Kinet Mech Cat* 133:209–227

13. Gou X, Okejiri F, Zhang ZH, Liu MM, Liu JX, Chen H, Chen KQ, Lu XY, Ouyang PK, Fu J (2020) Tannin-derived bimetallic CuCo/C catalysts for an efficient in-situ hydrogenation of lauric acid in methanol-water media. *Fuel Process Technol* 205:10
14. Zhang J, Huo X, Li Y, Strathmann TJ (2019) Catalytic hydrothermal decarboxylation and cracking of fatty acids and lipids over Ru/C. *ACS Sustain Chem Eng* 7:14400–14410
15. Lange JP (2015) Renewable feedstocks: the problem of catalyst deactivation and its mitigation. *Angew Chem Int Ed* 54:13186–13197
16. Ravenelle RM, Schüßler F, D'Amico A, Danilina N, Van Bokhoven JA, Lercher JA, Jones CW, Sievers C (2010) Stability of zeolites in hot liquid water. *J Phys Chem C* 114:19582–19595
17. Zhang ZH, Chen H, Wang CX, Chen KQ, Lu XY, Ouyang PK, Fu J (2018) Efficient and stable Cu–Ni/ZrO<sub>2</sub> catalysts for in situ hydrogenation and deoxygenation of oleic acid into heptadecane using methanol as a hydrogen donor. *Fuel* 230:211–217
18. Wei J, Wang G, Chen F, Bai M, Liang Y, Wang HT, Zhao DY, Zhao YX (2018) Sol-Gel synthesis of metal-phenolic coordination spheres and their derived carbon composites. *Angew Chem Int Ed* 57:9838–9843
19. Wang Q, Li H, Chen LQ, Huang XJ (2001) Monodispersed hard carbon spherules with uniform nanopores. *Carbon* 39:2211–2214
20. Sun XM, Li YD (2004) Colloidal carbon spheres and their core/shell structures with noble-metal nanoparticles. *Angew Chem Int Ed* 43:597–601
21. Yang WP, Li XX, Li Y, Zhu RM, Pang H (2019) Applications of metal-organic-framework-derived carbon materials. *Adv Mater* 31:35
22. Shi YT, Ai L, Shi HN, Gu XY, Han YJ, Chen JX (2022) Carbon-coated Ni–Co alloy catalysts: preparation and performance for in-situ aqueous phase hydrodeoxygenation of methyl palmitate to hydrocarbons using methanol as the hydrogen donor. *Front Chem Sci Eng* 16:443–460
23. Shi HN, Gu XY, Shi YT, Wang DD, Shu SH, Wang ZZ, Chen JX (2023) Efficient hydrothermal deoxygenation of methyl palmitate to diesel-like hydrocarbons on carbon encapsulated Ni–Sn intermetallic compounds with methanol as hydrogen donor. *Front Chem Sci Eng* 17:139–155
24. Gu X, Shi H, Wang D, Chen J (2022) Glucose-derived carbon-coated Ni–In intermetallic compounds for in situ aqueous phase selective hydrogenation of methyl palmitate to hexadecanol. *React Kinet Mech Cat* 135:1621–1634
25. Indra A, Song T, Paik U (2018) Metal organic framework derived materials: progress and prospects for the energy conversion and storage. *Adv Mater* 30:25
26. Li XX, Zheng SS, Jin L, Li Y, Geng PB, Xue HG, Pang H, Xu Q (2018) Metal-organic framework-derived carbons for battery applications. *Adv Energy Mater* 8:25
27. Chen LY, Wang HF, Li CX, Xu Q (2020) Bimetallic metal-organic frameworks and their derivatives. *Chem Sci* 11:5369–5403
28. Tian FP, Ru QF, Qiao CX, Sun X, Jia CY, Wang Y, Zhang YF (2019) Adsorption desulfurization of model gasoline by metal-organic framework Ni<sub>3</sub>(BTC)<sub>2</sub>. *J Energy Chem* 32:8–14
29. Israr F, Chun D, Kim Y, Kim DK (2016) High yield synthesis of Ni-BTC metal-organic framework with ultrasonic irradiation: role of polar aprotic DMF solvent. *Ultrason Sonochem* 31:93–101
30. Dou ZS, Yu JC, Xu H, Cui YJ, Yang Y, Qian GD (2013) Facile preparation of continuous indium metal-organic framework thin films on indium tin oxide glass. *Thin Solid Films* 544:296–300
31. Volkringer C, Loiseau T (2006) A new indium metal-organic 3D framework with 1,3,5-benzenetricarboxylate, MIL-96 (In), containing  $\mu_3$ -oxo-centered trinuclear units and a hexagonal 18-ring network. *Mater Res Bull* 41:948–954
32. Liu P, Chen CZ, Zhou MH, Xu JM, Xia HH, Shang SB, Jiang JC (2021) Metal-organic framework-derived Ni-based catalyst for the hydrotreatment of triolein into green diesel. *Sustain Energy Fuels* 5:1809–1820
33. Chinthaginjala JK, Bitter JH, Lefferts L (2010) Thin layer of carbon-nano-fibers (CNFs) as catalyst support for fast mass transfer in hydrogenation of nitrite. *Appl Catal A* 383:24–32
34. Kim HC, Huh S (2020) Porous carbon-based supercapacitors directly derived from metal-organic frameworks. *Materials* 13:74
35. Zhang C, Liao P, Wang H, Sun J, Gao P (2018) Preparation of novel bimetallic CuZn-BTC coordination polymer nanorod for methanol synthesis from CO<sub>2</sub> hydrogenation. *Mater Chem Phys* 215:211–220
36. Xia BY, Yan Y, Li N, Wu HB, Lou XW, Wang X (2016) A metal-organic framework-derived bifunctional oxygen electrocatalyst. *Nat Energy* 1:8



37. Aijaz A, Masa J, Rosler C, Xia W, Weide P, Botz AJR, Fischer RA, Schuhmann W, Muhler M (2016) Co@Co<sub>3</sub>O<sub>4</sub> encapsulated in carbon nanotube-grafted nitrogen-doped carbon polyhedra as an advanced bifunctional oxygen electrode. *Angew Chem Int Ed Engl* 55:4087–4091
38. Xia W, Zhu JH, Guo WH, An L, Xia DG, Zou RQ (2014) Well-defined carbon polyhedrons prepared from nano metal-organic frameworks for oxygen reduction. *J Mater Chem A* 2:11606–11613
39. Qian YH, Hu ZG, Ge XM, Yang SL, Peng YW, Kang ZX, Liu ZL, Lee JY, Zhao D (2017) A metal-free ORR/OER bifunctional electrocatalyst derived from metal-organic frameworks for rechargeable Zn-Air batteries. *Carbon* 111:641–650
40. Miao C, Marin-Flores O, Dong T, Gao DF, Wang Y, Garcia-Perez M, Chen SL (2018) Hydrothermal catalytic deoxygenation of fatty acid and bio-oil with in situ H<sub>2</sub>. *ACS Sustain Chem Eng* 6:4521
41. Miao C, Marin-Flores O, Davidson SD, Li TT, Dong T, Gao DF, Wang Y, Garcia-Perez M, Chen SL (2016) Hydrothermal catalytic deoxygenation of palmitic acid over nickel catalyst. *Fuel* 166:302–308
42. Yeh TM, Hockstad RL, Linic S, Savage PE (2015) Hydrothermal decarboxylation of unsaturated fatty acids over PtSn<sub>x</sub>/C catalysts. *Fuel* 156:219–224
43. Yao XY, Strathmann TJ, Li YL, Cronmiller LE, Ma HL, Zhang J (2021) Catalytic hydrothermal deoxygenation of lipids and fatty acids to diesel-like hydrocarbons: a review. *Green Chem* 23:1114–1129
44. Yang Y, Dong H, Wang Y, He C, Wang Y, Zhang X (2018) Synthesis of octahedral like Cu-BTC derivatives derived from MOF calcined under different atmosphere for application in CO oxidation. *J Solid State Chem* 258:582–587
45. Mondal S, Singuru R, Shit SC, Hayashi T, Irle S, Hijikata Y, Mondal J, Bhaumik A (2018) Ruthenium nanoparticle-decorated porous organic network for direct hydrodeoxygenation of long-chain fatty acids to alkanes. *ACS Sustain Chem Eng* 6:1610–1619

**Publisher's Note** Springer Nature remains neutral with regard to jurisdictional claims in published maps and institutional affiliations.

Springer Nature or its licensor (e.g. a society or other partner) holds exclusive rights to this article under a publishing agreement with the author(s) or other rightsholder(s); author self-archiving of the accepted manuscript version of this article is solely governed by the terms of such publishing agreement and applicable law.